

# All-Optical Silicon Modulators Based on Carrier Injection by Two-Photon Absorption

Christina Manolatu, *Member, IEEE*, and Michal Lipson, *Member, IEEE, Member, OSA*

**Abstract**—This paper presents a theoretical analysis of a silicon all-optical modulator based on free-carrier injection by two-photon absorption (TPA) in a highly light-confining structure. In spite of the weak optoelectronic properties of silicon, strong light confinement allows high modulation depths in very compact devices requiring low-energy pump pulses. This analysis is applied to 1-5  $\mu\text{m}$  radius silicon ring resonators with the pump pulse coupled on-chip and including in the model the scattering loss due to sidewall roughness originating from the fabrication process. The calculations show that using this scheme, modulation depths greater than 80% can be achieved, with no more than 3 pJ of pump pulse energy, at speeds on the order of 10 GHz.

**Index Terms**—All-optical modulation, free-carrier plasma effect, ring resonators, two-photon absorption.

## I. INTRODUCTION

ALL-OPTICAL switches and modulators, where light is controlled by light, enable ultrafast signal processing by overcoming the limitations of optical-to-electronic conversion. In particular, all-optical control on a silicon chip is of great importance toward developing highly integrated optical communication components because of the potential for monolithic integration of optics on CMOS-compatible platforms [1]. Silicon photonic structures that bend, split, couple, and filter light have recently been demonstrated [2]; however, in these structures, the flow of light cannot be modified. For active or tunable waveguide devices, the complex effective index of the structure must be varied in order to produce phase or intensity modulation. Because the optical Kerr effect is very weak in silicon [3], the preferred mechanism for achieving fast index changes is the free-carrier plasma dispersion effect [4], [5]. In all-optical devices, free carriers are generated by linear (single-photon) absorption or two-photon absorption (TPA) of an intense pump beam that thereby controls the flow of a weak probe signal. However, the large indirect bandgap, small TPA coefficient [3], and weak index dependence on free-carrier concentration [5] make all-optical control in silicon very challenging. Consequently, most all-optical Silicon devices demonstrated to date require intense pump beams, out-of-plane excitation, or large

Manuscript received November 23, 2004; revised November 29, 2005. This work was supported by the Semiconductor Research Corporation under Grant 2005-RJ-1296, the Cornell Center for Nanoscale Systems, the Cornell Center for Material Research under CCMR Grant M23-8494, the STC program of the National Science Foundation (NSF) under Agreement DMR-0120967, the NSF's CAREER Grant 0446571, and Gernot Pomrenke of the Air Force Office of Scientific Research under Grants F49620-03-1-0424 and FA9550-05-C-0102.

The authors are with the Department of Electrical and Computer Engineering, Cornell University, Ithaca, NY 14853 USA (e-mail: m1292@cornell.edu).  
Digital Object Identifier 10.1109/JLT.2005.863326

sizes, and are not suitable for monolithic integration on-chip [6]–[10].

The limitations of silicon as an optoelectronic material can be overcome using resonant structures that strongly confine light. The field enhancement inside a high-finesse resonator and the strong wavelength dependence of the transmission can increase the modulation effects by orders of magnitude. This principle has been demonstrated using ring resonators in III–V materials [11]–[13] and more recently in silicon [14], [15]. Such devices are suitable for monolithic integration when the pump beam is coupled into the system through the same on-chip waveguides as the probe beam. In silicon, this can be achieved using the Raman effect [16]–[21], the Kerr effect [22], or TPA [15]. Here, we concentrate on the strongest of these effects, TPA, significant around 1550 nm, which allows excitation of free carriers by pump photons with energies well below the bandgap. In this paper, we analyze the performance and dynamics of silicon all-optical modulators for different regimes of excitation and degree of light confinement.

This paper is organized as follows. In Section II, we introduce waveguide-based resonators as building blocks for all-optical modulators. In Section III, we discuss the mechanisms for all-optical modulation in silicon. In Section IV, the dynamic analysis of a resonator-based all-optical modulator under short pulse excitation is presented and is applied to specific examples of ring resonators. Finally, our conclusions are presented in Section V.

## II. RESONATORS AS MODULATORS

Resonators are ideal building blocks for all-optical modulators because of their compactness, strong light confinement, and wavelength sensitivity. Traveling wave resonators such as ring and disk resonators are particularly attractive due to their simplicity and very low bending losses achievable with miniature sizes (radii 1–5  $\mu\text{m}$ ) in high index contrast systems [23]. In this section, we show the effects of light confinement in a resonator on the degree of modulation. The basic structure considered here consists of a ring resonator of radius  $R$  evanescently coupled to a single waveguide as shown in the schematic in Fig. 1(a).

The amplitude of the field coupled into the ring resonator waveguide is given by

$$A_r = \frac{-j\kappa A_i}{1 - \sqrt{1 - \kappa^2} e^{-j\hat{\beta}(\omega)L}} \quad (1a)$$

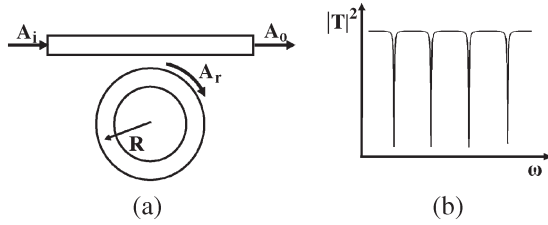


Fig. 1. (a) Schematic of a ring resonator side coupled to a waveguide. (b) General shape of the transmission spectrum.

where  $A_i$  is the input field amplitude in the waveguide. The output field amplitude in the waveguide is given by

$$A_o = \sqrt{1 - \kappa^2} A_i - j\kappa A_r e^{-j\tilde{\beta}(\omega)L} \quad (1b)$$

where  $L = 2\pi R$  is the roundtrip length of the cavity,  $\kappa$  is the coupling coefficient, and  $\tilde{\beta}(\omega) = \beta(\omega) - j\alpha_o/2$  is the complex propagation constant. In (1a) and (1b), the field amplitudes are normalized so that  $|A_i|^2$  and  $|A_o|^2$  are the input and output powers, respectively, of the waveguide mode, and  $|A_r|^2$  is the power coupled into the ring waveguide. The transmission response of this resonant system is

$$T(\omega) \equiv \frac{A_o}{A_i} = \frac{\sqrt{1 - \kappa^2} - e^{-j\tilde{\beta}(\omega)L}}{1 - \sqrt{1 - \kappa^2} e^{-j\tilde{\beta}(\omega)L}} \quad (2)$$

The resonance condition is  $\beta(\omega_{om})L = 2\pi m$ , where  $m$  is an integer, i.e., the ring circumference equals  $m$  guided wavelengths at  $\omega_{om}$ . At each resonance,  $|T(\omega)|^2$  has a minimum, with the value determined by the relation between  $\kappa$  and  $\alpha_o$ . Expanding  $\beta(\omega)$  to first order around a resonance frequency  $\omega_o$  as  $\beta(\omega) = \beta(\omega_o) + (\omega - \omega_o)/v_g$ , where  $v_g$  is the group velocity, we can express the transmission response (2) as a periodic function of  $\omega$  with free spectral range  $\Delta\omega_{FSR} = 2\pi v_g/L$ . The general shape of the transmission spectrum is shown in Fig. 1(b). For small roundtrip loss ( $\alpha_o L \ll 1$ ), weak coupling ( $\kappa^2 \ll 1$ ), and frequencies  $\omega - \omega_o \ll \omega_o$ , (1) and (2) can be written as

$$a_r = \frac{-j\sqrt{r_e}}{j(\omega - \tilde{\omega}_o) + \frac{r_e}{2}} A_i \quad (3a)$$

$$A_o = A_i - j\sqrt{r_e} a_r \quad (3b)$$

$$T(\omega) = \frac{j(\omega - \tilde{\omega}_o) - \frac{r_e}{2}}{j(\omega - \tilde{\omega}_o) + \frac{r_e}{2}} \quad (4)$$

where  $\tilde{\omega}_o = \omega_o + jr_o/2$  is the complex resonance frequency, with  $r_o = \alpha_o v_g$  being the energy decay rate in the cavity due to absorption and scattering, and  $r_e = \kappa^2 v_g/L$  is the energy decay rate due to external coupling. The cavity photon lifetime is  $\tau_p = 1/(r_o + r_e)$ . The amplitude  $a_r$  in (3) is normalized so that  $|a_r|^2$  is the energy in the cavity mode. In a low-loss ring resonator, the amplitudes  $a_r$  and  $A_r$  are related by

$$|A_r|^2 = \frac{v_g}{L} |a_r|^2 \quad (5)$$

and  $|A_r|^2$  now represents the average mode power carried along the ring waveguide. This relation results from the fact

that the power of a waveguide mode is equal to its energy per unit length times the group velocity. Note that (3) and (4) describe any resonant system with a single coupling port. Working with the energy-normalized amplitude is more suitable for small low-loss resonators and leads to a simpler analysis that is independent of the exact geometry of the resonator [24], [25].

The full-width at half-maximum (FWHM) bandwidth of the Lorentzian responses in (3) and (4) is  $\Delta\omega_{FWHM} = 1/\tau_p$  and the total quality factor is  $Q = \omega_o/\Delta\omega_{FWHM}$ . The resonator finesse is defined as  $F = \Delta\omega_{FSR}/\Delta\omega_{FWHM}$ . On resonance, the power coupled into the ring is enhanced by  $|A_r/A_i|^2 = (\kappa F/\pi)^2$  and is maximized under the critical coupling condition [25], [26]

$$\sqrt{1 - \kappa^2} = e^{-\alpha_o L/2} \quad \text{or} \quad r_e \approx r_o. \quad (6)$$

Under this condition,  $T(\omega_o) = 0$ , i.e., on resonance the input power is completely extracted from the waveguide and transferred to the resonator with enhancement  $|A_r/A_i|^2 = F/\pi$ .

The transmission response of the resonant system is highly sensitive to the index of the resonator waveguide the stronger the light confinement in the resonator is. Therefore, efficient amplitude modulation is possible by changing the refractive index of the ring resonator. A small complex index change  $\Delta\tilde{n} = \Delta n - jc\Delta\alpha/2\omega_o$ , where  $\alpha$  is the material absorption, results in a small shift of the complex resonance frequency  $\Delta\tilde{\omega}_o = \Delta\omega_o + j\Delta r_o/2$ . This can be calculated using perturbation theory as

$$\Delta\tilde{\omega}_o = -\omega_o \frac{\iiint_V n \Delta\tilde{n} |\vec{E}|^2 dx dy dz}{\iiint_V n^2 |\vec{E}|^2 dx dy dz} \quad (7)$$

where  $V$  is the volume of the resonator, and  $V = LA$ , where  $A$  is the cross-sectional area of the ring waveguide core. The electric field in the ring waveguide has the form

$$\vec{E} = a_r \vec{e}(x, y) e^{-j\tilde{\beta}z} \quad (8)$$

with energy normalization

$$\frac{1}{2} \varepsilon_o \iiint_V n^2 |\vec{E}|^2 dx dy dz = |a_r|^2. \quad (9)$$

Here,  $z$  is defined along the ring circumference and  $x$  and  $y$  in the cross-section of the ring waveguide. Since  $\alpha_o L \ll 1$ , we can make the approximation  $\iiint_V dx dy dz \approx L \iint dx dy$ . If, in addition,  $n$  and  $\Delta\tilde{n}$  are uniform in the waveguide core, (7) can be written as follows. For the real part (resonance frequency shift)

$$\Delta\omega_o = -\omega_o \Gamma \frac{\Delta n}{n_r} \quad (10a)$$

and for the imaginary part (energy decay rate change)

$$\Delta r_o = \Gamma \frac{c\Delta\alpha}{n_r} \quad (10b)$$

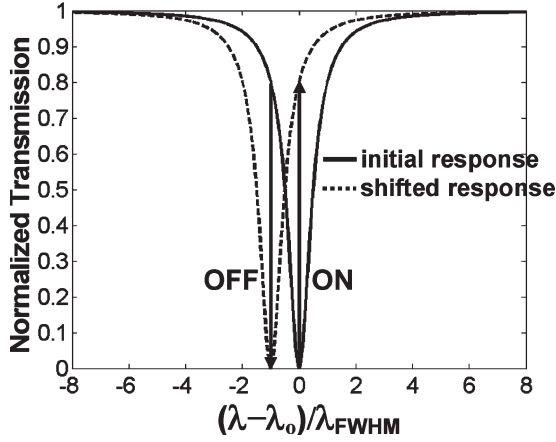


Fig. 2. Example showing the shift of the transmission spectrum for a ring resonance with  $Q = 4000$ , as a result of a refractive index change  $\Delta n \approx -0.001$  in the ring waveguide core.

where  $n_r$  is the value of  $n$  in the ring waveguide core, and  $\Gamma$  is the confinement factor defined here in terms of energy density as

$$\Gamma = \frac{\iint_A n^2 |\vec{e}(x, y)|^2 dx dy}{\iint_{\infty} n^2 |\vec{e}(x, y)|^2 dx dy}. \quad (11)$$

Equation (10a) shows that a small reduction of the refractive index blue-shifts the resonance. As seen in Fig. 2, this shift causes the transmission of a signal that is initially at or slightly above a resonant wavelength to change from a low to a high value (ON operation) and the transmission of an input signal that is initially below the resonant wavelength to change from a high to a low value (OFF operation). For the example in Fig. 2, we have considered a silicon ring critically coupled to a waveguide, with quality factor  $Q \approx \lambda_o / \Delta\lambda_{FWHM} = 4000$  and confinement factor  $\Gamma = 0.9$ , typical for Si/SiO<sub>2</sub> single-mode waveguides. Using (10a) with core index  $n_r = 3.48$ , we find that a refractive index change by  $\Delta n = -0.001$  can cause a spectral shift of  $\lambda_o \approx \Delta\lambda_{FWHM}$  and thus a change of the transmission of a probe signal at  $\lambda_{\text{probe}} = \lambda_o$  (ON operation) and  $\lambda_{\text{probe}} = \lambda_o - \Delta\lambda_{FWHM}$  (OFF operation) by more than 80% as shown in Fig. 2.

### III. MODULATION MECHANISM IN SILICON

Due to the weak nonlinearity of silicon, the preferred mechanism for changing the refractive index at high speed is the free-carrier plasma dispersion effect. This effect causes a (linear) change in the refractive index and the absorption according to [5]

$$\Delta n^L = -8.8 \times 10^{-22} \Delta N - 8.5 \times 10^{-18} (\Delta P)^{0.8} \quad (12a)$$

$$\Delta \alpha^L = 8.5 \times 10^{-18} \Delta N + 6.0 \times 10^{-18} \Delta P \quad (12b)$$

where  $\Delta N$  and  $\Delta P$  are the free electron and hole concentrations, respectively, in cm<sup>-3</sup>. These changes result in a linear shift of the complex resonance frequency of a cavity by  $\Delta\tilde{\omega}_o^L =$

$\Delta\omega_o^L + j\Delta r_o^L/2$ , according to (7) or (10). Since  $\Delta n^L < 0$ , the free-carrier plasma effect always blue-shifts the resonance.

The required free-carrier concentration can be generated electrically or optically. In all-optical applications, free carriers are generated by a pump beam with sufficient photon energy and intensity. The resulting index and absorption changes cause modulation of the transmission of a weak probe signal. The mechanism of free-carrier photo-excitation is either linear (single-photon) or nonlinear (two-photon) absorption (TPA) of the pump photons.

All-optical modulation using a silicon microring resonator can be achieved in a compact device that is suitable for monolithic integration, where the pump beam is coupled into the resonator through the same silicon waveguide and in the same wavelength range as the probe signal [15]. Due to silicon's transparency in telecom wavelengths, this pump scheme can only be employed with Raman, Kerr, or TPA, which is the strongest of these effects. In silicon, TPA is significant at around 1550 nm, allowing excitation of free carriers with photon energies well below the bandgap. This mechanism also causes small nonlinear index and absorption changes  $\Delta n^{\text{NL}}$  and  $\Delta \alpha^{\text{NL}}$ , respectively, which are given by

$$\Delta n^{\text{NL}} = n_{2I} I_{\text{pump}} \quad (13a)$$

$$\Delta \alpha^{\text{NL}} = \beta_{\text{TPA}} I_{\text{pump}} \quad (13b)$$

where  $n_{2I} = 0.79 \text{ cm}^2/\text{W}$ , and  $\beta_{\text{TPA}} = 0.45 \times 10^{-13} \text{ cm/GW}$  are the Kerr and TPA coefficients, respectively, of silicon reported in [3].  $I_{\text{pump}}$  is the pump intensity coupled into the ring given by  $I_{\text{pump}} = 1/2c\epsilon_o n |\vec{E}^{\text{pump}}|^2$ , where the pump field  $\vec{E}^{\text{pump}}$  has the form of (8) with amplitude  $a_r^{\text{pump}}$ .

Substituting (13a) and (13b) in (7) with the assumption of uniform core refractive index and normalization (9), we can write the nonlinear contributions to  $\Delta\tilde{\omega}_o$  as

$$\Delta\omega_o^{\text{NL}} = -\omega_o \frac{cn_{2I} |a_r^{\text{pump}}|^2}{n_r^2 V_{\text{eff}}} \quad (14a)$$

$$\Delta r_o^{\text{NL}} = \beta_{\text{TPA}} \frac{c^2 |a_r^{\text{pump}}|^2}{n_r^2 V_{\text{eff}}} \quad (14b)$$

where  $V_{\text{eff}}$  is the effective volume. With the approximation  $\iiint dx dy dz \approx L \iint dx dy$ ,  $V_{\text{eff}} = LA_{\text{eff}}$ , where  $A_{\text{eff}}$  is the effective area defined here in terms of energy density as

$$A_{\text{eff}} = \frac{\left[ \iint_{\infty} n^2 |\vec{e}(x, y)|^2 dx dy \right]^2}{\iint_A n^4 |\vec{e}(x, y)|^4 dx dy}. \quad (15)$$

In (14) and (15), we have assumed for simplicity that the pump and probe beams have approximately the same field distribution over  $x, y$ , as is the case when the two beams are near the same resonance frequency.

Since  $\Delta n^{\text{NL}} > 0$ , the Kerr effect causes a small red-shift of the resonance; however,  $|\Delta\omega_o^{\text{NL}}| \ll |\Delta\omega_o^L|$ , so the blue shift

dominates. The free-carrier concentration  $\Delta N = \Delta P \equiv N_{fc}$  in (12) is generated by TPA according to the rate equation

$$\frac{dN_{fc}}{dt} = \frac{1}{2\hbar\omega_{\text{pump}}} \Delta r_o^{NL} \frac{|a_r^{\text{pump}}|^2}{V} - \frac{N_{fc}}{\tau_{fc}} \quad (16)$$

where  $\hbar\omega_{\text{pump}}$  is the pump photon energy, and  $\tau_{fc}$  is the free-carrier lifetime. In general,  $\tau_p \ll \tau_{fc}$ , so the modulation speed is determined by the carrier lifetime. In [14] and [15], the value for  $\tau_{fc}$ , which is obtained from pump and probe experiments in a silicon ring with 5- $\mu\text{m}$  radius, is about 400 ps: much shorter than typical bulk silicon values. This short lifetime is attributed to fast recombination mechanisms on the unpassivated sidewalls of the structures and can be further shortened by shrinking the cavity size, manipulating the degree of surface passivation or by ion implantation [27].

As discussed in Section II, the enhancement of the pump power coupled from the waveguide into the resonator is proportional to the finesse. Since the finesse of Si/SiO<sub>2</sub> ring resonator systems is a few tens, the input pump power required for a given carrier concentration can be reduced by at least an order of magnitude compared with a nonresonant structure. Ignoring the weak Kerr effect in the example in Section II, the index change needed for detuning the resonance by  $\Delta\lambda_{\text{FWHM}}$  is achieved by a free-carrier concentration  $N_{fc} = 3.5 \times 10^{17} \text{ cm}^{-3}$ . In order to estimate the required pump power for modulation, we consider a Si/SiO<sub>2</sub> ring waveguide with cross-section  $0.48 \mu\text{m} \times 0.24 \mu\text{m}$  and  $\Gamma = 0.9$ ,  $A_{\text{eff}} = 0.14 \mu\text{m}^2$  at  $1.55 \mu\text{m}$  calculated from the modal field. The group index is  $n_g = 4.1$ , so the spectral range of a ring with  $R = 5 \mu\text{m}$  is  $\Delta\lambda_{\text{FSR}} = 18.65 \text{ nm}$  and the finesse is  $F \approx 48$ . Using (14b) and (5) in (16) at steady state ( $dN_{fc}/dt = 0$ ) with  $\tau_{fc} = 400 \text{ ps}$ , we find that the average pump power required inside the ring is 532 mW. This corresponds to an input pump power in the waveguide down to 35 mW due to power enhancement, which under critical coupling is equal to  $F/\pi \approx 15.28$ . This estimate is valid for pump pulses that are much longer than the free-carrier and cavity photon lifetimes. When very short pump pulses are used, the modulation effects are more accurately described by the full-dynamic analysis presented in the next section.

#### IV. DYNAMIC ANALYSIS OF RESONATOR-BASED ALL-OPTICAL MODULATORS

##### A. Theory

In high-speed all-optical modulation applications, the duration of the pump pulse is only a few picoseconds and is comparable to the cavity photon lifetime and much shorter than the free-carrier lifetime. Therefore, a full dynamic analysis must be performed in order to obtain the transient response of the system. In general, this is done by solving the nonlinear propagation equations for the pump and probe fields in the ring waveguide, coupled with the rate equation for the carrier concentration, for given pump and probe inputs [11], [12]. Such an approach takes into account both the temporal dependence and the spatial variation along the ring of all the quantities involved. In the work presented here, we are considering low-

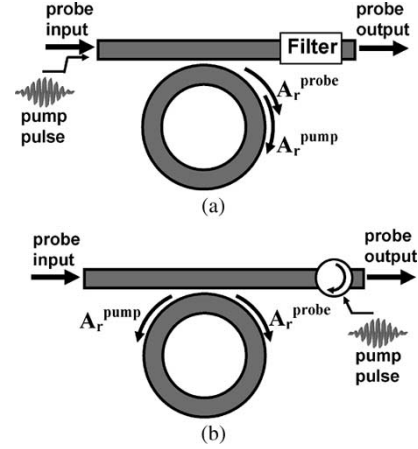


Fig. 3. Schematic of a modulator based on a ring resonator coupled to a waveguide with (a) pump and probe at different resonant wavelengths and coupled in the same direction and (b) pump and probe at the same resonant wavelength and coupled from opposite directions.

loss ring resonators with roundtrip times much shorter than the duration of the optical pulses. It is therefore possible to simplify the analysis by eliminating the spatial variation of the fields along the ring circumference based on the discussion in Section II. The dynamic behavior of the system is then expressed only in terms of the temporal variation of its optical and material properties.

In the analysis presented below, free carriers and nonlinear effects are generated only by the pump since the probe is much weaker, and there is no coupling between the two beams. The pump is a short pulse centered at a frequency  $\omega_{\text{pump}}$  and is assumed to have a Gaussian envelope with  $1/e$  width equal to  $\tau_{\text{pulse}}$ , while the probe is a weak continuous-wave signal at  $\omega_{\text{probe}}$ . Since  $\tau_{\text{pulse}}$  is only a few picoseconds, any thermal effects are neglected. If  $\omega_{\text{pump}}$  and  $\omega_{\text{probe}}$  are around two different resonances, the two signals can copropagate in the resonator and be separated at the output by a filter, as shown in Fig. 3(a). If, instead, the pump and the probe are around the same resonance, they can only be separated based on their direction of propagation, each being coupled to one of the two counter-propagating waves in the ring as shown in Fig. 3(b). Here, we consider the latter case with  $\omega_{\text{pump}}, \omega_{\text{probe}} \approx \omega_o$ , so we can assume that the two beams have approximately the same field distributions and therefore “see” the same coupling, loss, and confinement.

The rate equations for the energy-normalized pump and probe amplitudes in the cavity  $a_r^{\text{pump}}$  and  $a_r^{\text{probe}}$  can be derived from (3a) by setting  $j(\omega - \omega_{\text{pump}}) \rightarrow d/dt$  and  $j(\omega - \omega_{\text{probe}}) \rightarrow d/dt$ , respectively, and with the substitution  $\tilde{\omega}_o \rightarrow \omega_o + \Delta\omega_o^L + \Delta\omega_o^{NL} + j(r_o + \Delta r_o^L + \Delta r_o^{NL})/2$ .

$$\begin{aligned} \frac{d}{dt} a_r^{\text{pump}}(t) &= -j [\omega_{\text{pump}} - \omega_o - \Delta\omega_o^L(t) - \Delta\omega_o^{NL}(t)] a_r^{\text{pump}}(t) \\ &\quad - \frac{1}{2} [r_o + \Delta r_o^L(t) + \Delta r_o^{NL}(t)] a_r^{\text{pump}}(t) \\ &\quad - \frac{r_e}{2} a_r^{\text{pump}}(t) - j\sqrt{r_e} A_i^{\text{pump}}(t) \end{aligned} \quad (17a)$$

$$\begin{aligned}
 & \frac{d}{dt} a_r^{\text{probe}}(t) \\
 &= -j [\omega_{\text{probe}} - \omega_o - \Delta\omega_o^L(t) - \Delta\omega_o^{\text{NL}}(t)] a_r^{\text{probe}}(t) \\
 & \quad - \frac{1}{2} [r_o + \Delta r_o^L(t) + \Delta r_o^{\text{NL}}(t)] a_r^{\text{probe}}(t) \\
 & \quad - \frac{r_e}{2} a_r^{\text{probe}}(t) - j\sqrt{r_e} A_i^{\text{probe}}(t). \tag{17b}
 \end{aligned}$$

In (17),  $\Delta\omega_o^L(t)$  and  $\Delta r_o^L(t)$  are obtained from (10), where  $\Delta n^L$  and  $\Delta\alpha^L$  are given by (12) and the free-carrier concentration varies in time according to (16). The nonlinear changes  $\Delta\omega_o^{\text{NL}}(t)$  and  $\Delta r_o^{\text{NL}}(t)$  are obtained from (14). The output of interest in the transmitted probe amplitude is given as

$$A_o^{\text{probe}}(t) = A_i^{\text{probe}}(t) - j\sqrt{r_e} a_r^{\text{probe}}(t). \tag{18}$$

To calculate the complex resonance frequency as a function of time and the corresponding transmission spectrum, we integrate (17a) numerically coupled with (10), (12), (14), and (16). The transient transmission response given by (18) is obtained by numerical integration of (17b) to get  $a_r^{\text{probe}}(t)$ , using the newly obtained  $\tilde{\omega}_o$  at every time step.

### B. Examples

We now apply the above analysis to ring resonators of different sizes, critically coupled to a silicon waveguide. The purpose is to find the dependence of modulation depth and pump energy requirements on resonator size. We consider a silicon ring waveguide ( $n_{\text{Si}} = 3.48$ ) with  $\text{SiO}_2$  cladding ( $n_{\text{SiO}_2} = 1.46$ ) and with core dimensions  $0.48 \mu\text{m} \times 0.24 \mu\text{m}$ . Using a mode solver configured for analyzing ring resonators [28], we obtain the resonance frequency, scattering loss, confinement factor, and effective area for ring radii 1–5  $\mu\text{m}$ .

Ideally, the bending loss for such high index contrast waveguides is negligible for radii down to about 1.5  $\mu\text{m}$ , but, in practice, surface roughness originating from the fabrication process causes scattering loss that reduces  $Q$ . To account for this in our numerical model, we include absorption at the sidewalls such that the quality factor of the uncoupled resonator  $Q_o = \omega_o/r_o$  for a 5- $\mu\text{m}$  radius ring is approximately 7500 (under critical coupling  $Q = Q_o/2$ ). This value is consistent with the measurements in [14] and [15] for similar ring resonators. In order to analyze the effect of bending and scattering loss on light confinement, we calculate certain basic resonator parameters as a function of ring radius. The results are shown in Fig. 4(a) and (b), where it can be seen that quality and confinement factors do not change noticeably when the radius is reduced down to 2  $\mu\text{m}$ , while the resonance shifts to longer wavelengths. As the ring radius becomes smaller than 2  $\mu\text{m}$ , the quality and confinement factors drop significantly, reducing the wavelength sensitivity and the finesse of the resonator. We will therefore examine rings with radii 2–5  $\mu\text{m}$ .

For given resonator and pump pulse parameters and free-carrier lifetime, there are two optimal probe wavelengths—one for ON and one for OFF operation—that lead to maximum modulation of the transmitted signal. To obtain them, we take the difference  $\Delta|T|^2$  between the transmission spectrum at the

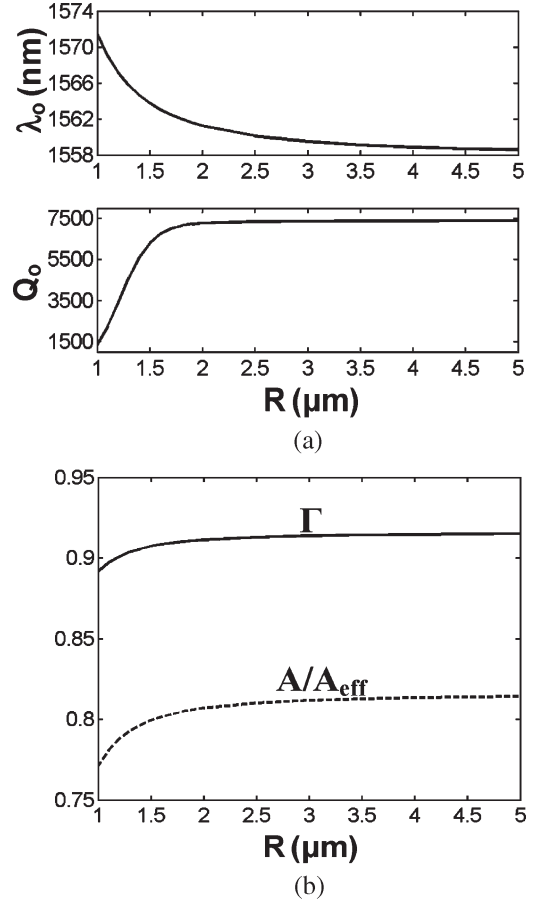


Fig. 4. (a) Resonant wavelength and quality factor of the uncoupled resonator. (b) Confinement factor and effective area as a function of radius for Si/SiO<sub>2</sub> ring resonators with waveguide cross-section 0.48  $\mu\text{m} \times 0.24 \mu\text{m}$ .

moment of maximum blue shift of the resonance, and the transmission spectrum in the absence of the pump.  $\Delta|T|^2$  is a function of wavelength with a maximum above  $\lambda_o$  and a minimum below  $\lambda_o$ , corresponding to optimal probe wavelengths for ON and OFF operations, respectively. As maximum modulation increases, the optimal wavelength moves closer to  $\lambda_o$  in the ON case and further away from  $\lambda_o$  in the OFF case. This is shown in the example in Fig. 5, where  $\Delta|T|^2$  has been plotted as a function of  $\lambda_{\text{probe}} - \lambda_o$  for a critically coupled ring with radius 5  $\mu\text{m}$  and different pump pulse energies  $E_p$  when  $\lambda_{\text{pump}} = \lambda_o$ ,  $\tau_{\text{pulse}} = 12$  ps (FWHM  $\approx 20$  ps), and  $\tau_{fc} = 400$  ps. We rely on such curves to determine the optimal probe wavelengths and corresponding modulation in all the examples below.

Modulation depth is defined here as

$$\text{MD} = \frac{(|T|_{\text{max}}^2 - |T|_{\text{min}}^2)}{|T|_{\text{max}}^2}. \tag{19}$$

Fig. 6 shows the maximum MD (i.e., at the optimal probe wavelength) as a function of pump pulse energy for different ring radii. From this graph, it is clear that a reduction of the ring size significantly lowers the pump energy required to achieve a given modulation depth since, with  $Q$  being roughly the same, the power enhancement factor is inversely proportional to the ring size. This is illustrated in the transient responses in Fig. 7.

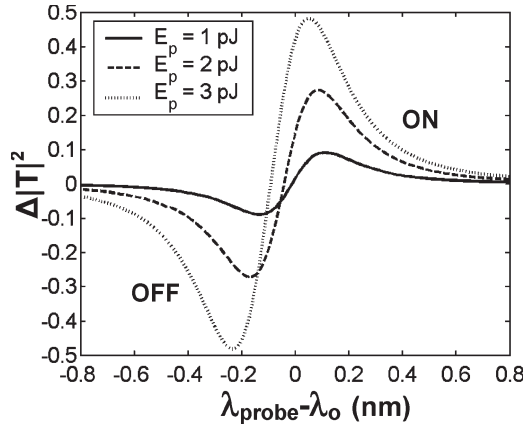


Fig. 5. Difference of the transmission spectra at the point of maximum spectral blue shift for different pump pulse energies  $E_p$  as a function of the deviation of the probe from the initial resonant wavelength of a  $5\text{-}\mu\text{m}$  radius ring.

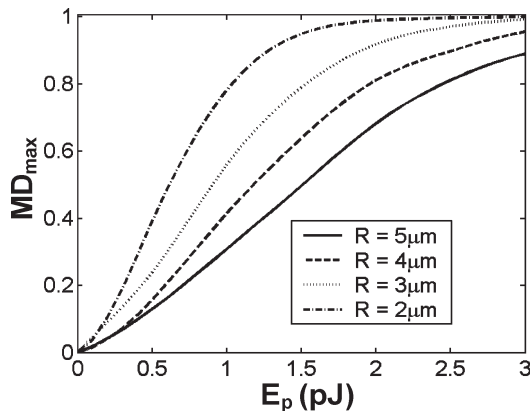


Fig. 6. Maximum modulation depth as a function of pump pulse energy for different ring radii, showing the effect of resonator size.

In each case in Fig. 7, the pump has  $\lambda_{\text{pump}} = \lambda_o$  and  $\tau_{\text{pulse}} = 12$  ps, and the probe is chosen for maximum ON ( $\lambda_{\text{probe}} - \lambda_o \approx 0.06$  nm) and OFF modulation ( $\lambda_{\text{probe}} - \lambda_o \approx -0.23$  nm), where  $\lambda_o = 1558.6$  nm for the  $5\text{-}\mu\text{m}$  radius and  $\lambda_o = 1561.24$  nm the  $2\text{-}\mu\text{m}$  radius ring. We can see that the pump energy required for achieving approximately the same transient response is almost proportional to the ring radius, i.e.,  $E_p = 3$  pJ for  $R = 5$   $\mu\text{m}$  and  $E_p = 1.25$  pJ for  $R = 2$   $\mu\text{m}$  when  $\tau_{fc} = 400$  ps. The modulation depth as defined in (19) is  $MD \approx 90\%$ . The corresponding maximum resonance wavelength shifts are  $\Delta\lambda_o \approx -0.176$  nm and  $\Delta\lambda_o \approx -0.183$  nm, and the peak values of the free-carrier concentration are  $N_{fc} \approx 1.04 \times 10^{17} \text{ cm}^{-3}$  and  $1.09 \times 10^{17} \text{ cm}^{-3}$ . The dissipated pump energy that generates the required free carriers by TPA is only 0.1 pJ for  $R = 5$   $\mu\text{m}$  and 0.042 pJ for  $R = 2$   $\mu\text{m}$ , which is almost proportional to the ring radius. These values are consistent with the estimates obtained from the experimental result in [15], i.e., 0.12 pJ for  $MD > 90\%$  in a  $5\text{-}\mu\text{m}$  ring.

Since cavity lifetime and pump pulse are much shorter than the free-carrier lifetime, the latter determines the modulation speed. The value  $\tau_{fc} = 400$  ps in our examples is based on previous experimental results on Si ring resonators [14], [15] and is much shorter than in bulk Si. This is attributed primarily to fast recombination mechanisms on the unpassivated sidewalls

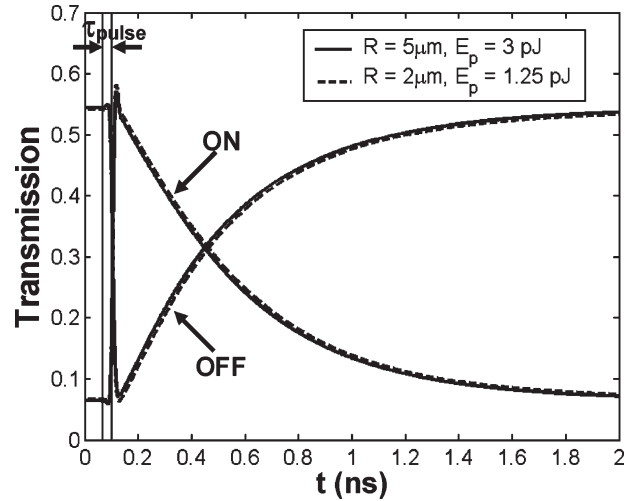


Fig. 7. Transient transmission responses in ON and OFF operation for rings of radius 2 and  $5$   $\mu\text{m}$  and probe wavelengths chosen for maximum modulation in each case.

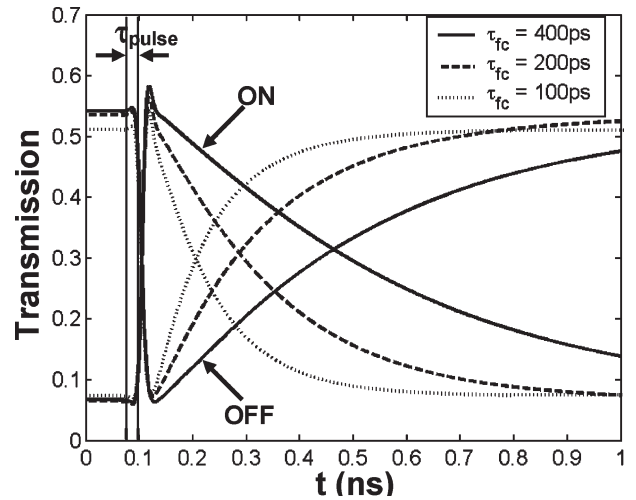


Fig. 8. Transient responses for ON and OFF operation at optimal probe wavelengths with pump energy 1.25 pJ and different carrier lifetimes in a critically coupled ring resonator of radius  $2$   $\mu\text{m}$ .

of these structures. A further reduction of  $\tau_{fc}$  and increase of the modulation speed are possible by shrinking the cavity size, manipulating surface passivation, or by using ion implantation [27]. Since the pump pulse is much shorter than  $\tau_{fc}$ , reducing the carrier lifetime is not expected to significantly affect the concentration of free carriers and, consequently, the modulation depth. This is shown in Fig. 8, where transient responses have been plotted for a critically coupled ring of  $2\text{-}\mu\text{m}$  radius and free-carrier lifetimes  $\tau_{fc} = 400$ , 200, and 100 ps. The pump pulse is the same as in previous examples, and the optimal probe wavelengths have been used for each free-carrier lifetime.

The small dips and peaks observed in the ON and OFF responses, respectively, coinciding with the pump pulse duration, are due to the weak Kerr effect, which instantaneously shifts the transmission spectrum in the opposite direction than the free-carrier plasma effect. An additional peak appears in the ON curves only, right after the expiration of the pump pulse. This is attributed to the very fast release into the waveguide of the

energy that was stored in the resonator before the arrival of the pump pulse in a time scale comparable to the resonator lifetime.

## V. CONCLUSION

Using a simplified theoretical model suitable for small low-loss resonators, we have analyzed the modulation performance of a ring-resonator-based silicon all-optical modulator. Our results have shown that in spite of the weak optoelectronics properties of silicon, highly confining microcavities enable fast all-optical modulation with very low pump energies and bandwidth determined by the free-carrier lifetime. Shrinking the cavity size without compromising the quality factor can significantly lower the pump energy required for certain modulation depths. This principle applies to any type of highly confined microcavities. For example, using high- $Q$  photonic crystal microcavities with sub-micrometer modal volumes (as opposed to several micrometers of the rings), we can expect a further reduction of the required energy for a given modulation depth. Furthermore, our results show that it is possible to increase the modulation speed by reducing the free-carrier lifetime without compromising the modulation depth.

## REFERENCES

- [1] R. A. Soref, "Silicon-based optoelectronics," *Proc. IEEE*, vol. 81, no. 12, pp. 1687–1706, Dec. 1993.
- [2] K. Wada, H. C. Luan, C. Lim, and D. R. L. C. Kimerling, "On-chip interconnection beyond semiconductor roadmap: Silicon microphotonics," in *Proc. SPIE—Int. Soc. Opt. Eng.*, Boston, MA, 2002, vol. 4870, pp. 437–443.
- [3] M. Dinu, F. Quochi, and H. Garcia, "Third-order nonlinearities in silicon at telecom wavelengths," *Appl. Phys. Lett.*, vol. 82, no. 18, pp. 2954–2956, May 2003.
- [4] R. A. Soref, "Electrooptical effects in silicon," *IEEE J. Quantum Electron.*, vol. QE-23, no. 1, pp. 123–129, Jan. 1987.
- [5] R. A. Soref and B. R. Bennett, "Kramers–Kronig analysis of electro-optical switching in silicon," in *Proc. SPIE*, Cambridge, MA, 1987, vol. 704, pp. 32–37.
- [6] N. D. Sankey, D. F. Prelewitz, and T. G. Brown, "All-optical switching in a nonlinear periodic-waveguide structure," *Appl. Phys. Lett.*, vol. 12, no. 23, pp. 1427–1429, Mar. 1992.
- [7] A. Hache and M. Bourgeois, "Ultrafast all-optical switching in a silicon-based photonic crystal," *Appl. Phys. Lett.*, vol. 77, no. 25, pp. 4089–4091, Dec. 2000.
- [8] F. Z. Henari, K. Morgenstern, W. J. Blau, V. A. Karavanskii, and V. S. Dneprovskii, "Third-order optical nonlinearity and all-optical switching in porous silicon," *Appl. Phys. Lett.*, vol. 67, no. 3, pp. 323–325, Jul. 1995.
- [9] C. Z. Zhao, G. Z. Li, E. K. Liu, Y. Gao, and X. D. Liu, "Silicon on insulator Mach–Zehnder waveguide interferometers operating at 1.3  $\mu\text{m}$ ," *Appl. Phys. Lett.*, vol. 67, no. 17, pp. 2448–2449, Oct. 1995.
- [10] S. Stepanov and S. Ruschin, "Modulation of light by light in silicon-on-insulator waveguides," *Appl. Phys. Lett.*, vol. 83, no. 25, pp. 5151–5153, Dec. 2003.
- [11] V. Van, T. A. Ibrahim, K. Ritter, P. P. Absil, F. G. Johnson, R. Grover, J. Goldhar, and P.-T. Ho, "All-optical nonlinear switching in GaAs–AlGaAs microring resonators," *IEEE Photon. Technol. Lett.*, vol. 14, no. 1, pp. 74–76, Jan. 2002.
- [12] V. Van, T. A. Ibrahim, P. P. Absil, F. G. Johnson, R. Grover, and P.-T. Ho, "Optical signal processing using nonlinear semiconductor microring resonators," *IEEE J. Sel. Topics Quantum Electron.*, vol. 8, no. 3, pp. 705–713, May/June 2002.
- [13] T. A. Ibrahim, W. Cao, Y. Kim, J. Li, J. Goldhar, P.-T. Ho, and C. H. Lee, "All-optical switching in a laterally coupled microring resonator by carrier injection," *IEEE Photon. Technol. Lett.*, vol. 15, no. 1, pp. 36–38, Jan. 2003.
- [14] V. R. Almeida, C. A. Barrios, R. R. Panepucci, M. Lipson, M. A. Foster, D. G. Ouzounov, and A. L. Gaeta, "All-optical switching on a silicon chip," *Opt. Lett.*, vol. 29, no. 24, pp. 2867–2869, Dec. 2004.
- [15] V. R. Almeida, C. A. Barrios, R. R. Panepucci, and M. Lipson, "All-optical control of light on a silicon chip," *Nature*, vol. 431, no. 7012, pp. 1081–1084, Oct. 2004.
- [16] Q. Xu, V. R. Almeida, and M. Lipson, "Time-resolved study of Raman gain in highly confined silicon-on-insulator waveguides," *Opt. Express*, vol. 12, no. 19, pp. 4437–4442, Sep. 2004.
- [17] R. L. Espinola, J. I. Dadap, R. M. Osgood, Jr., S. J. McNab, and Y. A. Vlasov, "Raman amplification in ultrasmall silicon-on-insulator wire waveguides," *Opt. Express*, vol. 12, no. 16, pp. 3713–3718, Aug. 2004.
- [18] T. K. Liang and H. K. Tsang, "On Raman gain in silicon waveguides: Limitations from two-photon-absorption generated carriers," in *Proc. Conf. Lasers and Electro-Optics (CLEO)*, San Francisco, CA, May 2004, vol. 2, p. 2.
- [19] O. Boyraz and B. Jalali, "Demonstration of a silicon Raman laser," *Opt. Express*, vol. 12, no. 21, pp. 5269–5273, Oct. 2004.
- [20] R. Jones, H. Rong, A. Liu, A. W. Fang, M. J. Paniccia, D. Hak, and O. Cohen, "Net continuous wave optical gain in a low loss silicon-on-insulator waveguide by stimulated Raman scattering," *Opt. Express*, vol. 13, no. 2, pp. 519–525, Jan. 2005.
- [21] H. Rong, A. Liu, R. Jones, O. Cohen, D. Hak, R. Nicolaescu, A. Fang, and M. Paniccia, "An all-silicon Raman laser," *Nature*, vol. 433, no. 7023, pp. 292–294, Jan. 2005.
- [22] H. M. van Driel, S. W. Leonard, H.-W. Tan, A. Birner, J. Schilling, S. L. Schweizer, R. B. Wehrspohn, and U. Gosele, "Tuning 2D photonic crystals," in *Proc. SPIE*, Denver, CO, Aug. 2004, vol. 5511, pp. 1–9, n. 1.
- [23] Y. A. Vlasov and S. J. McNab, "Losses in single-mode silicon-on-insulator strip waveguides and bends," *Opt. Express*, vol. 12, no. 8, pp. 1622–1631, Apr. 2004.
- [24] H. A. Haus, *Waves and Fields in Optoelectronics, Chapter*. Englewood Cliffs, NJ: Prentice-Hall, 1984.
- [25] B. E. Little, S. T. Chu, H. A. Haus, J. Foresi, and J.-P. Laine, "Microring resonator channel-dropping filters," *J. Lightw. Technol.*, vol. 15, no. 6, pp. 998–1005, Jun. 1997.
- [26] A. Yariv, "Universal relations for coupling of optical power between microresonators and dielectric waveguides," *Electron. Lett.*, vol. 36, no. 4, pp. 321–322, Feb. 2000.
- [27] A. Chin, K. Y. Lee, B. C. Lin, and S. Horng, "Picosecond photoresponse of carriers in Si ion-implanted Si," *Appl. Phys. Lett.*, vol. 69, no. 5, pp. 653–655, Jul. 1996.
- [28] M. Popovic, "Complex-frequency leaky mode computations using PML boundary layers for dielectric resonant structures," *Integr. Photon. Res., Trends Opt. Photon. Series*, vol. 91, pp. 143–145, Jun. 2003.

**Christina Manolatu** (S'97–M'01) was born in Greece. She received the Ph.D. degree from the Massachusetts Institute of Technology (MIT), Cambridge, in 2001, focusing on theoretical analysis and numerical modeling of integrated optical structures.

After a postdoctoral position at MIT, she joined the Cornell Nanophotonics Group, Cornell University, Ithaca, NY, in 2003 as a Visiting Scientist.

**Michal Lipson** (M'02) received the B.S., M.S., and Ph.D. degrees in physics from the Technion—Israel Institute of Technology, Haifa, Israel.

In December 1998, she joined the Department of Material Science and Engineering, Massachusetts Institute of Technology (MIT), Cambridge, as a Postdoctoral Associate. She joined the School of Electrical and Computer Engineering, Cornell University, Ithaca, NY, in 2001 as an Assistant Professor. Her research at Cornell University involves novel on-chip nanophotonics devices. She is the author of over 100 papers in major research journals and conferences in physics and optics.

Dr. Lipson is the Chair for the Integrated Optics Technical Group, OSA, and is the Topical Editor of *Optics Letters*. She was the recipient of the National Science Foundation (NSF) Career award in 2004.